

ATM: IMPROVING MODEL MERGING BY ALTERNATING TUNING AND MERGING

Luca Zhou* Daniele Solombrino* Donato Crisostomi Maria Sofia Bucarelli
Fabrizio Silvestri Emanuele Rodolà

Sapienza University of Rome

zhou.2135393@studenti.uniroma1.it
{solombrino, crisostomi, rodola}@di.uniroma1.it
{bucarelli, fsilvestri}@diag.uniroma1.it

ABSTRACT

Model merging has recently emerged as a cost-efficient paradigm for multi-task learning. Among current approaches, task arithmetic (Ilharco et al., 2022) stands out for its simplicity and effectiveness. In this paper, we motivate the effectiveness of task vectors by linking them to multi-task gradients. We show that in a single-epoch scenario, if the optimization is performed via gradient descent, task vectors are after one step mathematically equivalent to the gradients obtained via gradient descent in a multi-task setting, and still approximate these gradients in subsequent epochs. Furthermore, we show that the effectiveness of task vectors is largely driven by the first epoch’s gradient. Given this parallel between task vectors and gradients, we propose viewing model merging as a single step in an iterative process that Alternates between Tuning and Merging (ATM). We then propose two ways to utilize ATM. The first is to replace multi-task learning with ATM in scenarios where data sharing is prohibited (e.g. federated learning). The second is to improve the outcome of any model merging algorithm by applying a few post-hoc iterations of ATM on a small validation dataset, which is commonly available for hyperparameter tuning. Finally, we provide both empirical and theoretical support for the effectiveness of ATM, demonstrating that it minimizes an upper bound on the loss obtained by jointly finetuning all tasks.

1 INTRODUCTION

The pretrain-and-finetune paradigm has become the standard for many deep learning tasks, where a model pretrained on large-scale, unlabeled data is adapted to a specific downstream task with minimal tuning. However, when working with multiple tasks, a major drawback is the need to store separate finetuned models at inference. Model merging addresses this challenge by combining task-specific models into a single model capable of handling all tasks. This significantly reduces storage costs, as the unified model’s size remains comparable to that of a single-task model, regardless of the number of tasks. Among numerous model merging frameworks, *task arithmetic* (Ilharco et al., 2022) stands out for its simplicity and effectiveness. Given a pretrained model θ_0 and a model θ_i finetuned on task t_i , the *task vector* $\tau_i = \theta_i - \theta_0$ is defined as the difference between the finetuned and pretrained weights. For multi-task learning with n tasks, task arithmetic sums the n task vectors, scales the sum with a coefficient α , and adds the resulting vector back to the pretrained model.

In this paper, we explain the effectiveness of task arithmetic by linking task vectors to the gradients of the task losses. We start by noticing: when a model is finetuned for a single epoch using gradient descent (GD), the corresponding task vector is the additive inverse of the loss gradient, scaled by the learning rate. Similarly, the multi-task vector, obtained by summing individual task vectors, is equivalent to the additive inverse of the *average* loss gradient. Thus, task addition is analogous to performing a GD step on the sum of the average task losses. When finetuning spans multiple epochs, this equality becomes an approximation, with an error dependent on the learning rate.

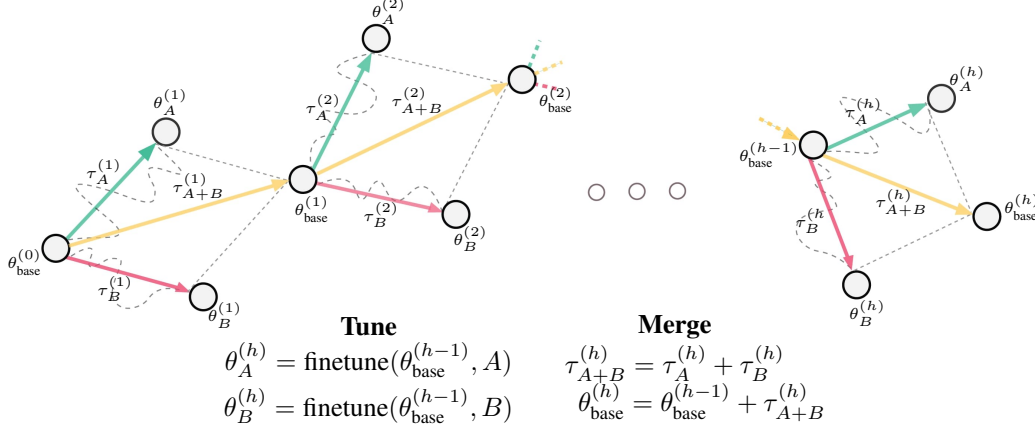


Figure 1: The ATM method, illustrated up to iteration h with two tasks (A and B). In each iteration, the **Tune** step finetunes the pretrained model $\theta_{\text{base}}^{(0)}$ separately on both tasks, and the **Merge** step aggregates the task vectors and applies the resulting multi-task vector to the base model. This process repeats, with each iteration using the updated model as the new base, continuing until a stopping condition is met.

While the single-epoch assumption is not always exact, we confirm that the first epoch contributes most to the gradient norm. Even when it does not, subsequent gradients tend to align with the first, confirming that the initial direction predominantly dictates the task vector’s effectiveness.

In this view, aggregation and merging in task arithmetic correspond to a noisy GD step when finetuning jointly on all tasks, using the sum of the average losses as the objective. In practice, this implies that the one-step nature of these techniques likely leads to overshooting the multi-task optimum, as they effectively perform GD on a multi-task dataset with a single, noisy step. The scaling factors optimized via the validation set essentially act as the learning rates in this process.

Building on these insights, we propose viewing task arithmetic as a single step in an iterative framework and introduce Alternating Tuning and Merging (ATM) – a generic framework that iteratively alternates between finetuning and merging. We propose applying ATM in two ways. The first is PA-ATM (Privacy-Aware ATM), which replaces multi-task learning in scenarios where multi-task data sharing is forbidden (e.g. federated learning). The second is PH-ATM (Post-Hoc ATM), which enhances any multi-task model by applying a few post-hoc iterations of ATM on a small set of validation data, which is commonly available and used for hyperparameter tuning. The flexibility of ATM enables the integration of any conflict-resolution method in the task arithmetic literature for further gains.

Finally, we rigorously prove that if gradient descent is adopted, then ATM iterations implicitly optimize the upper bound of a hypothetical multi-task model trained jointly on the datasets of all tasks.

To summarize, our contribution is four-fold:

- (i) We show that, under specific conditions, task vectors are equivalent to or approximate the gradients of the corresponding task losses.
- (ii) We introduce Alternating Tuning and Merging (ATM), a generic framework that generalizes task arithmetic and facilitates more gradual multi-task knowledge integration. Its flexibility allows it to incorporate any conflict-resolution method for further gains.
- (iii) We propose two ways of applying ATM in practice depending on the constraints. The first (PA-ATM) replaces multi-task learning where data sharing is forbidden, whereas the second (PH-ATM) is a post-hoc enhancement of any multi-task model.
- (iv) We mathematically prove that throughout the execution of ATM, the evolving base model reduces the loss of a multi-task model finetuned on all tasks jointly.

2 TASK VECTORS AS GRADIENTS

In this section, we formally define the relationship between task vectors and task-loss gradients.

Theorem 1. Let $\{\theta_t^{(k)}\}_{t=1}^{|T|}$ be a set of models obtained by finetuning the base model θ_{base} for k epochs on tasks T using GD with a learning rate η , where finetuning task $t \in T$ minimizes the loss $\bar{L}_t(\theta) = \frac{1}{n_t} \sum_{i=1}^{n_t} \ell(x_i, y_i, \theta)$. Additionally, let $\{\tau_t^{(k)}\}_{t=1}^{|T|}$ denote the corresponding set of task vectors, with each $\tau_t^{(k)} = \theta_t^{(k)} - \theta_{base}$. Let $\tau_{MT}^{(k)}$ be the multi-task vector $\tau_{MT}^{(k)} = \sum_{t \in T} \tau_t^{(k)}$. Finally, let $\theta_{MT}^{(k)}$ represent the model obtained by minimizing the combined loss $\sum_{i=1}^{|T|} \bar{L}_i$ for k epochs using GD with a learning rate of $\alpha\eta$. It holds that

$$\tau_{MT}^{(1)} = -\eta \nabla \sum_{t \in T} \bar{L}_t(\theta_{base}) \quad (1)$$

$$\tau_{MT}^{(k)} = -\eta \sum_{t \in T} \sum_{j=0}^{k-1} \nabla \bar{L}_t(\theta_{MT}^{(j)}) + \frac{\eta^2}{2} C(\{\theta_{MT}^{(j)}\}_{j=1}^{k-2}) + O(\eta^3) \quad (2)$$

with

$$C(\{\theta_{MT}^{(j)}\}_{j=1}^h) = \sum_{t \in T} \sum_{\ell=0}^h \nabla^2 \bar{L}_t(\theta_{MT}^{(\ell)}) \sum_{m=0}^{\ell} \left[\alpha \sum_{t' \neq t, t' \in T} \nabla \bar{L}_{t'}(\theta_{MT}^{(m)}) + (\alpha - 1) \nabla \bar{L}_t(\theta_{MT}^{(m)}) \right] \quad (3)$$

We provide the proof in Appendix A.1. To better appreciate the relationship between a task vector and the gradient computed on the corresponding task dataset, consider the single-task case, where the task vector is exactly the additive inverse of the gradient, scaled by the learning rate η .

Remark 1. From Theorem 1, it follows that, for a single task t , and after a single finetuning epoch,

$$\tau_t = -\eta \nabla \bar{L}_t(\theta_{base}) \quad (4)$$

where η is the learning rate.

This implies that, under the theorem’s assumptions, adding the task vector to the pretrained model approximates the effect of finetuning the model; the same intuition applies to the multi-task case.

In fact, in Fig. 2 we report evidence that the multi-task model obtained by merging models finetuned for a *single* epoch performs competitively to the one obtained by merging models finetuned to convergence across all tasks. In other words, *for the sake of multi-task model merging, performing one epoch of finetuning is often enough, being the task vectors better approximations of the gradients.* Further discussion can be found in appendix C.

We formalize this through the following corollary.

Corollary. Let $\theta_{TA}^{(k)} = \theta_{base} + \alpha \sum_{t=1}^T \tau_t^{(k)}$ be the model obtained using vanilla task arithmetics. Using the same notation of Theorem 1, it holds that

$$\theta_{TA}^{(1)} = \theta_{MT}^{(1)} \quad (5)$$

$$\theta_{TA}^{(k)} = \theta_{MT}^{(k)} + \frac{\eta^2}{2} C(\{\theta_{MT}^{(j)}\}_{j=1}^{k-2}) + O(\eta^3) \quad \text{for } k > 1 \quad (6)$$

The corollary indicates that for $k > 1$, the multi-task vector still approximates the gradient of a model finetuned for the same number of epochs via GD, with an error on the order of $o(\eta^2)$. Despite the lack of exact equivalence, the effectiveness of task vectors still holds and can be explained by the fact that most of the model’s finetuning trajectory is driven by the gradient from the first epoch.

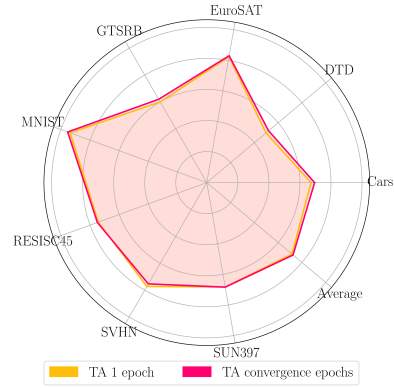


Figure 2: Task arithmetic accuracy: 1 epoch vs. convergence finetuning

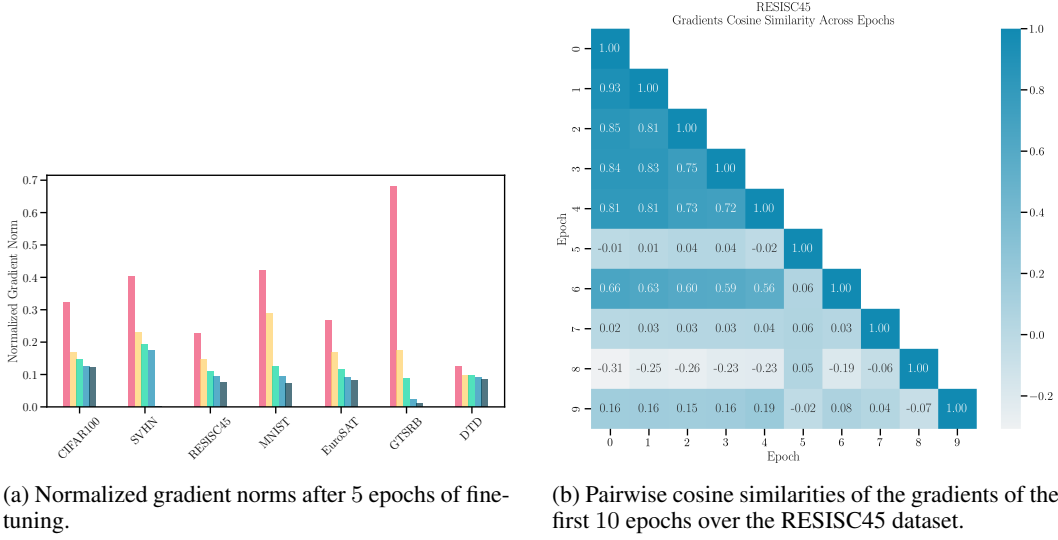


Figure 3: Analysis of gradient norms and alignment.

In Fig. 3a we plot the epoch-wise normalized gradient norm $\frac{\|\nabla_{\theta}^{(k)} L\|}{\sum_{k'=1}^K \|\nabla_{\theta}^{(k')} L\|}$. We observe that the first epoch contributes the most, accounting for up to 70% of the total gradient norms across all epochs. In cases where this is not true, such as with the RESISC45 dataset, we speculate that the direction is still largely determined by the first epoch. As depicted in Fig. 3b, the gradients from the first 5 epochs maintain a high cosine similarity (> 0.8) with the first epoch's gradient.

It is worth noting that this analysis does not exactly apply when optimizers like Adam are used instead of GD. However, treating Adam as an approximation to GD preserves intuition. From this view, reducing task interference corresponds to minimizing gradient conflicts in multi-task learning.

3 ATM: ALTERNATING TUNING AND MERGING

Building upon the insights of Section 2, we argue that task arithmetic is an approximation to a single GD step over the union of all the tasks. Following this parallel, we advocate taking further update steps iteratively.

The overall framework of ATM is depicted in Fig. 1. Specifically, we start from an initial base model $\theta_{\text{base}}^{(0)}$, we finetune it separately on each task to obtain the first-iteration task vectors $\tau_1^{(1)}, \dots, \tau_{|T|}^{(1)}$.

These are then aggregated and added to the base model to form the next-iteration unified model $\theta_{\text{base}}^{(1)}$. The procedure is iterated according to the following equation:

$$\theta_{\text{base}}^{(k+1)} = \theta_{\text{base}}^{(k)} + \frac{\alpha}{|T|} \sum_{t \in T} \tau_t^{(k)} \quad \forall k = 0, \dots, K-1. \quad (7)$$

The k -th iteration task vector for task t is obtained as $\tau_t^{(k)} = \theta_t^{(k)} - \theta_{\text{base}}^{(k)}$, where $\theta_t^{(k)}$ is a model obtained finetuning the k -th iteration base model $\theta_{\text{base}}^{(k)}$ on task t . The total number of iterations K can be predefined or based on a stop condition.

In practice, each iteration of ATM involves finetuning the current base model on all $|T|$ tasks using their task-specific data, thereby obtaining $|T|$ task vectors. These task vectors approximate the true task-specific directions the current base model should follow in order to attain enhanced performance on the corresponding tasks.

ATM's merging step at a given iteration consists of adding the mean of current-iteration task vectors to the current base model, although its flexibility allows any interference-resolution method in the task vector literature to be integrated. This step is intended to pull the base model closer to the multi-task basin on the loss landscape. Taking the average over T ensures that the magnitude of the update

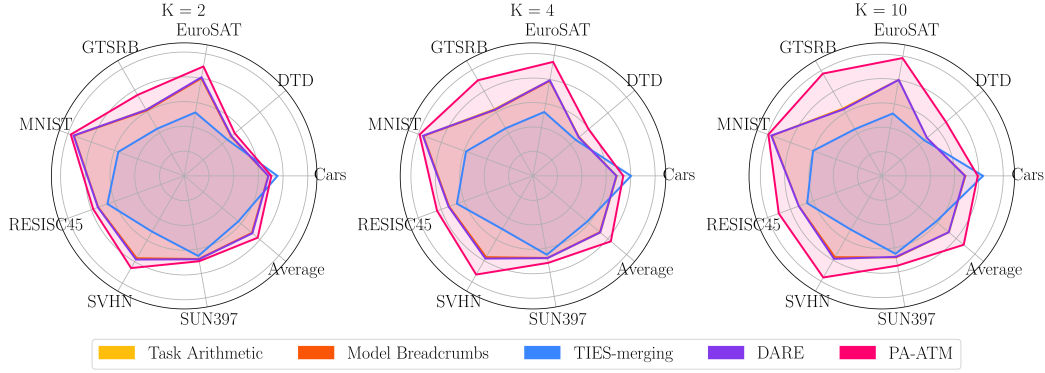


Figure 4: PA-ATM vs Baselines as computational budget K varies.

remains insensitive to the number of tasks. Note that the task vectors from previous iterations can be safely discarded after each iteration. Therefore, at any iteration, ATM only stores the current base model and one task vector for each of the $|T|$ tasks, incurring no additional storage requirements compared to task arithmetic.

ATM is generic and can be applied in numerous ways. One way is to build a multi-task model from scratch using non-centralized training data (**PA-ATM**) and a pretrained initialization. This tightly relates to *FedAVG* (McMahan et al., 2017) in the scenario of federated learning. The other way is to improve an existing merged model with a small set of validation data (**PH-ATM**). The difference between the two lies in the model initialization $\theta_{\text{base}}^{(0)}$ and data usage.

3.1 PA-ATM UPPER BOUNDS THE MULTI-TASK LOSS

We now show that a single PA-ATM step under GD minimizes the mean of average losses (\bar{L}_i) across tasks and prove that, under certain conditions, reducing this objective also decreases the loss of a model trained jointly on all datasets. As in Section 2, we assume GD is used for optimizing the model parameters. This assumption removes the stochasticity of the random sampling, enabling a more straightforward analysis while still providing insights into the dynamics of the optimization process. This section provides a concise overview; the detailed derivation is given in Appendix A.2.

We denote with t both the task and its corresponding dataset, whose cardinality is n_t . The total number of samples for all tasks is given by $N = \sum_{t \in T} n_t$. Inspired by Daheim et al. (2023), we define the *target loss* as the loss of a model trained jointly on all the datasets: $L_{\text{target}}(\theta) = \frac{1}{N} \sum_{i=1}^N \ell(x_i, y_i, \theta)$.

As detailed in Appendix A.2, when merging occurs after one step of finetuning on each dataset, the PA-ATM update corresponds to performing a GD step over the loss $L_{\text{PA-ATM}} = \frac{1}{|T|} \sum_{t \in T} \bar{L}_t$. Having established that one step of PA-ATM in GD minimizes L_{ATM} a key question follows: under what conditions does minimizing $L_{\text{PA-ATM}}$ also lead to a reduction in L_{target} ?

We show that if the drop in the PA-ATM loss exceeds a threshold, dependent on the sizes of the largest and smallest datasets whose losses respectively decrease and increase, then L_{target} - also decreases. In practice, this typically happens whenever the largest dataset’s loss decreases. A rigorous statement of the theorem and its derivation can be found in Appendix A.2.

4 EXPERIMENTS

4.1 EXPERIMENTAL SETTING

Datasets and Model The backbone model in all our experiments is the *ViT-B-16* (Dosovitskiy et al., 2021). We adhere to Ilharco et al. (2022) and compare PA-ATM and PH-ATM against the baselines on the the following image classification datasets: *DTD* (Cimpoi et al., 2014), *EuroSAT*

(Helber et al., 2019), *GTSRB* (Houben et al., 2013), *MNIST* (Lecun et al., 1998), *RESISC45* (Cheng et al., 2017), *SUN397* (Xiao et al., 2010), and *SVHN* (Netzer et al., 2011).

Baselines and Setup To gauge the performance of PA-ATM and PH-ATM, we consider several model merging baselines, including task arithmetic (TA) (Ilharco et al., 2022), TIES-merging (Yadav et al., 2023), model breadcrumbs (Davari & Belilovsky, 2023), and DARE (Yu et al., 2023). To ensure fair comparison across experiments, we adhere to the author-recommended hyperparameters whenever needed or available. Specifically, we adhere to Ilharco et al. (2022) and use AdamW (Loshchilov & Hutter, 2019) as the optimizer across all frameworks, including ours. For TIES-merging, we retain the top 15% of weights based on magnitude ranking. For model breadcrumbs, we set $\beta = 0.85$ and $\gamma = 0.993$. For DARE merging, we use a drop rate of 0.9. In all settings, we adopt mean aggregation of task vectors and use a scaling factor of 1 when applying them to the base model. For PA-ATM, we initialize the base model as the ViT-B-16 pretrained on ImageNet (Deng et al., 2009), whereas for PH-ATM, we initialize the base model as the multi-task model obtained from the application of task arithmetic. Note that while the goal of PA-ATM is to build a multi-task model from scratch, the goal of PH-ATM is to improve upon task arithmetic starting in the same conditions as the baseline conflict-resolution methods.

Strategy Following Ilharco et al. (2022), we evaluate all methods on the held-out test sets provided by each individual dataset and build the validation set by sampling 10% of the training set. We adopt classification *accuracy* as the evaluation metric, which is standard in the literature.

4.2 IMPACT OF EPOCH DISTRIBUTION ON PERFORMANCE

Throughout the paper, we adhered to the convention of merging after just a single epoch of finetuning during ATM iterations. One might question whether more epochs per merging step is beneficial. To show that the one-epoch convention is indeed optimal, we conduct the following experiment with PA-ATM. We establish a fixed compute budget of 10 finetuning epochs for each task, we then seek the optimal distribution of epochs among different numbers of ATM iterations. To exemplify, if 10 epochs are distributed among 5 iterations, then in each iteration a task is finetuned for 2 epochs.

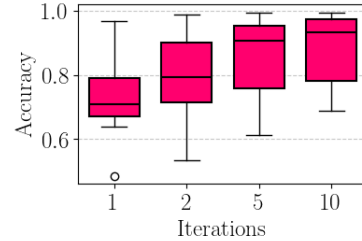


Figure 5: PA-ATM multi-task accuracy across budget distributions.

As depicted in Fig. 5, with a fixed compute budget, maximizing iterations while minimizing epochs per iteration yields the best results for ATM. This indicates that more gradual updates to the base model are preferable to abrupt ones. We observe a clear monotonous increase as more iterations are performed. Splitting 10 epochs across 10 iterations achieves the highest average accuracy of 88%, outperforming the 1 iteration of 10 epochs setting (analogous to task arithmetic) by around 16%. Detailed results can be found in the appendix 3. Therefore, the one-epoch convention holds and we subsequently adopt it by default.

4.3 EFFECT OF FINETUNING EPOCHS

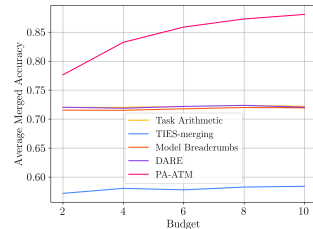


Figure 6: Average multi-task accuracy as budget varies.

We compare PA-ATM against baselines for different budgets of finetuning epochs. Specifically, we vary the total per-task finetuning epochs (K) within 2, 4, and 10 and compare the average test accuracy across tasks. As shown in Fig. 4, PA-ATM consistently outperforms the baselines for all budgets. Interestingly, while PA-ATM’s accuracy improves with more finetuning epochs, the baseline methods remain unaffected; see Fig. 6. In other words, *more specialization of the task-specific models does not necessarily benefit the one-shot unified multi-task model*. Detailed comparisons can be found in the appendix 2.

Method	Cars	DTD	EuroSAT	GTSRB	MNIST	RESISC45	SVHN	SUN397	Average
Pretrained	0.64	0.45	0.54	0.43	0.51	0.65	0.51	0.65	0.55
Finetuned	0.87	0.98	0.98	0.99	0.99	0.96	0.97	0.78	0.94
Task Arithmetic	0.69	0.52	0.83	0.62	0.95	0.75	0.75	0.68	0.73
TIES	0.88	0.45	0.44	0.41	0.63	0.63	0.42	0.63	0.56
Breadcrumbs	0.69	0.52	0.83	0.61	0.95	0.75	0.74	0.68	0.72
DARE	0.69	0.52	0.83	0.61	0.95	0.75	0.76	0.68	0.72
PH-ATM ₁₀	0.73	0.61	0.54	0.95	0.99	0.89	0.95	0.71	0.80
PA-ATM ₁₀	0.79	0.69	0.98	0.97	0.99	0.90	0.96	0.75	0.88
PA-ATM ₃₀	0.82	0.76	0.99	0.99	0.99	0.94	0.97	0.76	0.90

Table 1: Accuracy comparison under original baseline settings. PA-ATM₁₀ refers to PA-ATM employing 10 iterations.

4.4 COMPARISONS IN ORIGINAL SETTINGS

We compare the PA-ATM and PH-ATM to the baselines under their original data and hyperparameter setups, including author-specified epochs, weight decay, and learning rate warmup. With an abuse of notation for the sake of readability, the epochs for PH-ATM is based on validation data, unlike all other methods that use the training data. As illustrated in Table 1, PA-ATM unsurprisingly and significantly outperforms the baselines. With 10 iterations of ATM, it outperforms the best-performing baseline by 15% on average. If the budget is elevated to 30 iterations, the advantage grows to 17%.

We emphasize again that all baselines do make use of the validation data for hyperparameter tuning, while PH-ATM leverages it differently. Fig. 7 and Table 1 show that PH-ATM also outperforms the baselines across all tasks but one, with an average improvement of 7% over the best baseline. Thus, we postulate that estimating the task-proficiency directions through validation data, as done in PH-ATM, is a better option when further finetuning is allowed.

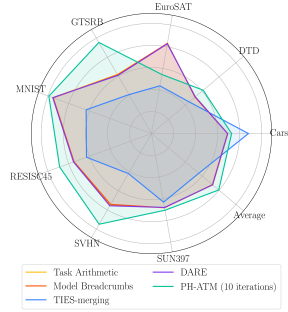


Figure 7: PH-ATM vs Baselines across all tasks but one.

5 DISCUSSION

5.1 EDUCATED TRAJECTORY

All baselines perform the aggregation step abruptly in an one-shot fashion over the initial pretrained checkpoint, likely overshooting the multi-task optimum. ATM variants, however, gradually traverses the loss landscape as the base model evolves, leading to more informed nudges toward the multi-task optimum. Fig. 8 depicts the 2D PCA projection of various merged checkpoints. Notably, TIES and Model Breadcrumbs, being deterministic post-hoc enhancement of task arithmetic, end up around the same suboptimal basin. DARE, on the other hand, is located far from the rest due to its stochastic pruning. PA-ATM and PH-ATM, however, start from different initializations and take gradual steps toward different and better basins, signaling the effectiveness of iterative merging.

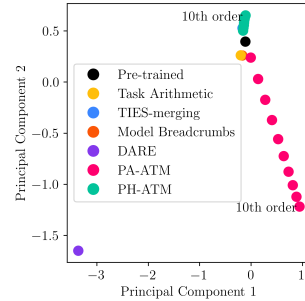


Figure 8: PCA of checkpoints

5.2 TASK PROFICIENCY IS NOT MERGEABILITY

Figures 6 and 2 show that task-specific expertise does not guarantee better multi-task performance. Stronger task-specific models attain higher task-specific specialization at the cost of deviating more from the gradient approximation; hence, the downstream performance is not a predictor of post-merging success. We hypothesize that highly specialized models diverge in parameter space, making abrupt one-shot merging suboptimal (Fig. 8). From a gradient perspective, this degradation occurs because vanilla task vectors approximate increasingly noisy multi-task gradients as finetun-

ing progresses. A lower degree of specialization keeps models closer to the pretrained checkpoint, as observed by [Ortiz-Jimenez et al. \(2024\)](#) in the tangent space, leading to less aggressive and more mergeable updates. This aligns with [Lu et al. \(2024\)](#), who attribute the issue to vanishing common knowledge in specialized models. Gradient approximation theory further supports this: fewer finetuning epochs yield better multi-task gradient approximations. ATM capitalizes on this by gradually integrating task-specific knowledge, ensuring less aggressive yet iterative merging. At each step, ATM task vectors provide adaptive nudges to the base model without reverting to the original pretrained checkpoint, unlike baseline methods.

5.3 LIMITATIONS OF ITERATIVE MERGING

Although ATM offers strong performance, its iterative nature exhibits drawbacks. It does not immediately provide task representations, as it iteratively generates vectors per task. However, it remains the best option for obtaining the best-performing multi-task model. We ensured a fair comparison by using the same finetuning epochs and data requirements and showed that a small validation set suffices. Lastly, ATM preserves a key advantage of task arithmetic: by generating task vectors independently, it avoids centralizing data, making it suitable for privacy-sensitive settings.

6 RELATED WORK

Mode Connectivity and Model Merging Mode connectivity explores how weights characterize local minima in the loss landscape. [Frankle et al. \(2020\)](#) studied linear mode connectivity in models with shared initialization, while [Entezari et al. \(2022\)](#) showed that models converge to a shared basin after resolving neuron permutations. Permutation-based merging leverages this insight to combine models without ensembling overhead. [Singh & Jaggi \(2020\)](#) proposed optimal-transport weight matching, [Git Re-Basin \(Ainsworth et al., 2022\)](#) introduced three rebasin variants, and [REPAIR \(Jordan et al., 2023\)](#) reduced barriers via activation renormalization. More recently, [Navon et al. \(2023\)](#) explored embedding-space merging, while [Crisostomi et al. \(2024\)](#) introduced cycle-consistent matching. For models with shared initialization, [Wortsman et al. \(2022\)](#) used simple averaging, while [Jolicoeur-Martineau et al. \(2023\)](#) aligned models to the population mean for stability. Weighted averaging approaches, such as RegMean ([Jin et al., 2022](#)) and Fisher-weighted averaging ([Matena & Raffel, 2021](#)), optimize merging weights based on specific criteria. [Daheim et al. \(2023\)](#) linked gradient mismatch to post-merging multi-task performance. Lastly, [Choshen et al. \(2022\)](#) proposed merging as an alternative to pretraining, arguing that a merged model can outperform any single fine-tuned checkpoint.

Task Vectors Task vector-based merging ([Ilharco et al., 2022](#)) finetunes a pretrained model on different tasks to obtain task vectors (differences between finetuned and original checkpoints). Arithmetic operations on these vectors enable forgetting, analogy learning, and multi-task learning. Several works aim to improve task vector merging by reducing task interference ([Deep et al., 2024](#); [Wang et al., 2024](#); [Huang et al., 2024](#)). Some methods include sparsifying task vectors or finetuning only lottery tickets ([Panda et al., 2024](#)). TIES-merging ([Yadav et al., 2023](#)) merges vectors by pruning, selecting a unified sign vector, and merging disjointly, while Model Breadcrumbs ([Davari & Belilovsky, 2023](#)) prunes both small and large-magnitude weights. DARE Merging ([Yu et al., 2023](#)) randomly masks out a portion of weights and scales up the rest. AdaMerging ([Yang et al., 2023](#)) optimizes aggregation coefficients, while [Yang et al. \(2024\)](#) proposed task-specific modules for test-time adaptation. [Ortiz-Jimenez et al. \(2024\)](#) introduced the concept of weight disentanglement and recommended finetuning in the tangent space. Unlike these one-shot methods, we propose an *iterative* approach that progressively refines the base model for better multi-task performance.

Federated Averaging PA-ATM is tightly related to Federated Averaging (FedAVG) ([McMahan et al., 2017](#)), as both alternate between local updates and aggregation while starting from a shared initialization. However, their underlying perspective differs. FedAVG is designed for distributed training on private, non-IID data, whereas PA-ATM focuses on model merging by iteratively integrating task-specific updates. In a sense, PA-ATM represents a bridge between model merging and federated learning which originate from two different purposes.

7 CONCLUSIONS

This paper connects task vectors to gradients in multi-task learning, forming the foundation for our proposed Alternating Tuning and Merging (ATM) framework. ATM iteratively refines model merging, addressing the shortcomings of one-shot methods. We introduce two practical frameworks: PA-ATM, which generalizes FedAVG and bridges model merging and federated learning, serving primarily for analysis, and PH-ATM, which enhances existing multi-task models using validation data only. Experiments on vision benchmarks confirm that ATM achieves strong performance with efficiency comparable to baselines. Our theoretical analysis further shows that PA-ATM optimizes an upper bound on the multi-task loss, providing insights into ATM’s effectiveness. The flexibility of ATM allows the additional integration of conflict-resolution and gradient-based techniques.

ETHICS STATEMENT

This research was conducted with a strong commitment to ethical standards in both data usage and experimental methodology. All datasets utilized in this study are publicly available. No personally identifiable information was accessed or used during the course of this research. Additionally, the experiments were designed to ensure fair comparisons across methods. We encourage future work that adheres to these same principles and addresses the broader societal impacts of machine learning.

REPRODUCIBILITY STATEMENT

We are committed to ensuring the reproducibility of our results and have taken steps to facilitate this for the broader research community. The code, datasets, and configurations used for the experiments in this paper are made available via a public repository. We are open to providing further instructions on the usage of our code. The hyperparameters, frameworks, and evaluation metrics have been thoroughly documented, and we provide clear descriptions of our experimental setup to allow for straightforward replication of our findings. We encourage the community to utilize these resources and provide feedback for further improvements.

ACKNOWLEDGMENTS

This work is supported by the ERC grant no.802554 (SPECGEO), PRIN 2020 project no.2020TA3K9N (LEGO.AI), and PNRR MUR project PE0000013-FAIR.

REFERENCES

- Samuel Ainsworth, Jonathan Hayase, and Siddhartha Srinivasa. Git Re-Basin: Merging models modulo permutation symmetries. In *The Eleventh International Conference on Learning Representations*, 2022.
- Gong Cheng, Junwei Han, and Xiaoqiang Lu. Remote sensing image scene classification: Benchmark and state of the art. *Proceedings of the IEEE*, 105(10), 2017.
- Leshem Choshen, Elad Venezian, Noam Slonim, and Yoav Katz. Fusing finetuned models for better pretraining. *ArXiv preprint*, abs/2204.03044, 2022. URL <https://arxiv.org/abs/2204.03044>.
- Mircea Cimpoi, Subhansu Maji, Iasonas Kokkinos, Sammy Mohamed, and Andrea Vedaldi. Describing textures in the wild. In *2014 IEEE Conference on Computer Vision and Pattern Recognition, CVPR 2014, Columbus, OH, USA, June 23-28, 2014*. IEEE Computer Society, 2014. doi: 10.1109/CVPR.2014.461. URL <https://doi.org/10.1109/CVPR.2014.461>.
- Donato Crisostomi, Marco Fumero, Daniele Baieri, Florian Bernard, and Emanuele Rodolà. c^2m^3 : Cycle-consistent multi-model merging. In *Advances in Neural Information Processing Systems*, volume 37, 2024.
- Nico Daheim, Thomas Möllenhoff, Edoardo Ponti, Iryna Gurevych, and Mohammad Emtiyaz Khan. Model merging by uncertainty-based gradient matching. In *Proc. ICLR*, 2023.

-
- MohammadReza Davari and Eugene Belilovsky. Model breadcrumbs: Scaling multi-task model merging with sparse masks. *ArXiv preprint*, abs/2312.06795, 2023. URL <https://arxiv.org/abs/2312.06795>.
- Pala Tej Deep, Rishabh Bhardwaj, and Soujanya Poria. Della-merging: Reducing interference in model merging through magnitude-based sampling. *ArXiv preprint*, abs/2406.11617, 2024. URL <https://arxiv.org/abs/2406.11617>.
- Jia Deng, Wei Dong, Richard Socher, Li-Jia Li, Kai Li, and Li Fei-Fei. Imagenet: A large-scale hierarchical image database. In *2009 IEEE Conference on Computer Vision and Pattern Recognition*, pp. 248–255, 2009. doi: 10.1109/CVPR.2009.5206848.
- Alexey Dosovitskiy, Lucas Beyer, Alexander Kolesnikov, Dirk Weissenborn, Xiaohua Zhai, Thomas Unterthiner, Mostafa Dehghani, Matthias Minderer, Georg Heigold, Sylvain Gelly, Jakob Uszkoreit, and Neil Houlsby. An image is worth 16x16 words: Transformers for image recognition at scale. In *9th International Conference on Learning Representations, ICLR 2021, Virtual Event, Austria, May 3-7, 2021*. OpenReview.net, 2021. URL <https://openreview.net/forum?id=YicbFdNTTy>.
- Rahim Entezari, Hanie Sedghi, Olga Saukh, and Behnam Neyshabur. The role of permutation invariance in linear mode connectivity of neural networks. In *The Tenth International Conference on Learning Representations, ICLR 2022, Virtual Event, April 25-29, 2022*. OpenReview.net, 2022. URL <https://openreview.net/forum?id=dNigytemkL>.
- Jonathan Frankle, Gintare Karolina Dziugaite, Daniel Roy, and Michael Carbin. Linear mode connectivity and the lottery ticket hypothesis. In *Proceedings of the 37th International Conference on Machine Learning, ICML 2020, 13-18 July 2020, Virtual Event*, volume 119 of *Proceedings of Machine Learning Research*. PMLR, 2020. URL <http://proceedings.mlr.press/v119/frankle20a.html>.
- Antonio Andrea Gargiulo, Donato Crisostomi, Maria Sofia Bucarelli, Simone Scardapane, Fabrizio Silvestri, and Emanuele Rodolà. Task singular vectors: Reducing task interference in model merging. *arXiv preprint arXiv:2412.00081*, 2024.
- Patrick Helber, Benjamin Bischke, Andreas Dengel, and Damian Borth. Eurosat: A novel dataset and deep learning benchmark for land use and land cover classification. *IEEE Journal of Selected Topics in Applied Earth Observations and Remote Sensing*, 12(7), 2019.
- Sebastian Houben, Johannes Stallkamp, Jan Salmen, Marc Schlipsing, and Christian Igel. Detection of traffic signs in real-world images: The German Traffic Sign Detection Benchmark. In *International Joint Conference on Neural Networks*, number 1288, 2013.
- Chenyu Huang, Peng Ye, Tao Chen, Tong He, Xiangyu Yue, and Wanli Ouyang. Emr-merging: Tuning-free high-performance model merging. *ArXiv preprint*, abs/2405.17461, 2024. URL <https://arxiv.org/abs/2405.17461>.
- Gabriel Ilharco, Marco Tulio Ribeiro, Mitchell Wortsman, Suchin Gururangan, Ludwig Schmidt, Hannaneh Hajishirzi, and Ali Farhadi. Editing models with task arithmetic. *The Eleventh International Conference on Learning Representations*, 2022.
- Xisen Jin, Xiang Ren, Daniel Preotiuc-Pietro, and Pengxiang Cheng. Dataless knowledge fusion by merging weights of language models. *ArXiv preprint*, abs/2212.09849, 2022. URL <https://arxiv.org/abs/2212.09849>.
- Alexia Jolicoeur-Martineau, Emy Gervais, Kilian Fatras, Yan Zhang, and Simon Lacoste-Julien. Population parameter averaging (papa). *ArXiv preprint*, abs/2304.03094, 2023. URL <https://arxiv.org/abs/2304.03094>.
- Keller Jordan, Hanie Sedghi, Olga Saukh, Rahim Entezari, and Behnam Neyshabur. REPAIR: RENormalizing permuted activations for interpolation repair. In *The Eleventh International Conference on Learning Representations*, 2023.
- Y. Lecun, L. Bottou, Y. Bengio, and P. Haffner. Gradient-based learning applied to document recognition. *Proceedings of the IEEE*, 86(11), 1998. doi: 10.1109/5.726791.

-
- Ilya Loshchilov and Frank Hutter. Decoupled weight decay regularization. In *International Conference on Learning Representations*, 2019. URL <https://openreview.net/forum?id=Bkg6RiCqY7>.
- Zhenyi Lu, Chenghao Fan, Wei Wei, Xiaoye Qu, Dangyang Chen, and Yu Cheng. Twin-merging: Dynamic integration of modular expertise in model merging. *arXiv preprint arXiv:2406.15479*, 2024.
- Michael Matena and Colin Raffel. Merging models with fisher-weighted averaging. 2021.
- Brendan McMahan, Eider Moore, Daniel Ramage, Seth Hampson, and Blaise Aguera y Arcas. Communication-efficient learning of deep networks from decentralized data. In *Artificial intelligence and statistics*, pp. 1273–1282. PMLR, 2017.
- Aviv Navon, Aviv Shamsian, Ethan Fetaya, Gal Chechik, Nadav Dym, and Haggai Maron. Equivariant deep weight space alignment, 2023.
- Yuval Netzer, Tao Wang, Adam Coates, Alessandro Bissacco, Baolin Wu, Andrew Y Ng, et al. Reading digits in natural images with unsupervised feature learning. In *NIPS workshop on deep learning and unsupervised feature learning*, volume 2011. Granada, 2011.
- Guillermo Ortiz-Jimenez, Alessandro Favero, and Pascal Frossard. Task arithmetic in the tangent space: Improved editing of pre-trained models. *Advances in Neural Information Processing Systems*, 36, 2024.
- Ashwinee Panda, Berivan Isik, Xiangyu Qi, Sanmi Koyejo, Tsachy Weissman, and Prateek Mittal. Lottery ticket adaptation: Mitigating destructive interference in llms. *ArXiv preprint*, abs/2406.16797, 2024. URL <https://arxiv.org/abs/2406.16797>.
- Sidak Pal Singh and Martin Jaggi. Model fusion via optimal transport. In Hugo Larochelle, Marc’Aurelio Ranzato, Raia Hadsell, Maria-Florina Balcan, and Hsuan-Tien Lin (eds.), *Advances in Neural Information Processing Systems 33: Annual Conference on Neural Information Processing Systems 2020, NeurIPS 2020, December 6-12, 2020, virtual*, 2020. URL <https://proceedings.neurips.cc/paper/2020/hash/fb2697869f56484404c8ceee2985b01d-Abstract.html>.
- Ke Wang, Nikolaos Dimitriadis, Guillermo Ortiz-Jimenez, François Fleuret, and Pascal Frossard. Localizing task information for improved model merging and compression. In *Forty-first International Conference on Machine Learning*, 2024.
- Mitchell Wortsman, Gabriel Ilharco, Samir Yitzhak Gadre, Rebecca Roelofs, Raphael Gontijo Lopes, Ari S. Morcos, Hongseok Namkoong, Ali Farhadi, Yair Carmon, Simon Kornblith, and Ludwig Schmidt. Model soups: averaging weights of multiple fine-tuned models improves accuracy without increasing inference time. In Kamalika Chaudhuri, Stefanie Jegelka, Le Song, Csaba Szepesvári, Gang Niu, and Sivan Sabato (eds.), *International Conference on Machine Learning, ICML 2022, 17-23 July 2022, Baltimore, Maryland, USA*, volume 162 of *Proceedings of Machine Learning Research*. PMLR, 2022. URL <https://proceedings.mlr.press/v162/wortsman22a.html>.
- Jianxiong Xiao, James Hays, Krista A. Ehinger, Aude Oliva, and Antonio Torralba. Sun database: Large-scale scene recognition from abbey to zoo. In *2010 IEEE Computer Society Conference on Computer Vision and Pattern Recognition*, pp. 3485–3492, 2010. doi: 10.1109/CVPR.2010.5539970.
- Prateek Yadav, Derek Tam, Leshem Choshen, Colin Raffel, and Mohit Bansal. Ties-merging: Resolving interference when merging models. 2023.
- Enneng Yang, Zhenyi Wang, Li Shen, Shiwei Liu, Guibing Guo, Xingwei Wang, and Dacheng Tao. Adamerging: Adaptive model merging for multi-task learning. In *The Twelfth International Conference on Learning Representations*, 2023.
- Enneng Yang, Li Shen, Zhenyi Wang, Guibing Guo, Xiaojun Chen, Xingwei Wang, and Dacheng Tao. Representation surgery for multi-task model merging. *ArXiv preprint*, abs/2402.02705, 2024. URL <https://arxiv.org/abs/2402.02705>.

Le Yu, Bowen Yu, Haiyang Yu, Fei Huang, and Yongbin Li. Language models are super mario: Absorbing abilities from homologous models as a free lunch. In *Forty-first International Conference on Machine Learning*, 2023.

A PROOFS

A.1 PROOFS OF THEOREM 1 AND COROLLARY 2

In this section, we provide proofs for Theorem 1 and Corollary 2. For clarity, we restate both the theorem and corollary.

Theorem. Let $\{\theta_t^{(k)}\}_{t=1}^{|T|}$ be a set of models obtained by finetuning the base model θ_{base} for k epochs on tasks T using GD with a learning rate η , where finetuning task $t \in T$ minimizes the loss $\bar{L}_t(\theta) = \frac{1}{n_t} \sum_{i=1}^{n_t} \ell(x_i, y_i, \theta)$. Additionally, let $\{\tau_t^{(k)}\}_{t=1}^{|T|}$ denote the corresponding set of task vectors, with each $\tau_t^{(k)} = \theta_t^{(k)} - \theta_{base}$. Let $\tau_{MT}^{(k)}$ be the multi-task vector $\tau_{MT}^{(k)} = \sum_{t \in T} \tau_t^{(k)}$. Finally, let $\theta_{MT}^{(k)}$ represent the model obtained by minimizing the combined loss $\sum_{i=1}^{|T|} \bar{L}_i$ for k epochs using GD with a learning rate of $\alpha\eta$. It holds that

$$\tau_{MT}^{(1)} = -\eta \nabla \sum_{t \in T} \bar{L}_t(\theta_{base}) \quad (8)$$

$$\tau_{MT}^{(k)} = -\eta \sum_{t \in T} \sum_{j=0}^{k-1} \nabla \bar{L}_i(\theta_{MT}^{(j)}) + \frac{\eta^2}{2} C(\{\theta_{MT}^{(j)}\}_{j=1}^{k-2}) + O(\eta^3) \quad (9)$$

with

$$C(\{\theta_{MT}^{(j)}\}_{j=1}^h) = \sum_{t \in T} \sum_{\ell=0}^h \nabla^2 \bar{L}_t(\theta_{MT}^{(\ell)}) \sum_{m=0}^{\ell} \left[\alpha \sum_{t' \neq t, t' \in T} \nabla \bar{L}_{t'}(\theta_{MT}^{(m)}) + (\alpha - 1) \nabla \bar{L}_t(\theta_{MT}^{(m)}) \right] \quad (10)$$

Corollary. Let $\theta_{TA}^{(k)} = \theta_{base} + \alpha \sum_{t=1}^T \tau_t^{(k)}$ be the model obtained using vanilla task arithmetics. Using the same notation of Theorem 1, it holds that

$$\theta_{TA}^{(1)} = \theta_{MT}^{(1)} \quad (11)$$

$$\theta_{TA}^{(k)} = \theta_{MT}^{(k)} + \frac{\eta^2}{2} C(\{\theta_{MT}^{(j)}\}_{j=1}^{k-2}) + O(\eta^3) \quad \text{for } k > 1 \quad (12)$$

We recall that $\theta_i^{(k)}$ is the model obtained by finetuning on task i for k epochs, and that both the finetuning on different tasks and the training on the average loss start from a pretrained model θ_{base} .

To prove the statement of the theorem and of the corollary we need an intermediate result. We introduce the following notation:

$$r_i(\theta) = \alpha \sum_{j \neq i} \nabla \bar{L}_j(\theta) + (\alpha - 1) \nabla \bar{L}_i(\theta) = \alpha \sum_{j=1}^{|T|} \nabla \bar{L}_j(\theta) - \nabla \bar{L}_i(\theta_{base}) \quad (13)$$

$$p_i^k(\theta_{base}, \theta_{MT}^{(1)}, \dots, \theta_{MT}^{(k)}) = \sum_{j=0}^k r_i(\theta_{MT}^{(j)}) \quad (14)$$

$$s_i^k(\theta_{base}, \dots, \theta_{MT}^{(k)}) = \sum_{j=0}^k \nabla^2 \bar{L}_i(\theta_{MT}^{(j)}) [p_i^j(\theta_{base}, \dots, \theta_{MT}^{(j-1)})]. \quad (15)$$

Lemma. Using the notation introduced in Theorem 1, it holds that

$$\theta_i^{(1)} = \theta_{MT}^{(1)} + \eta p_i^0(\theta_{base}) \quad (16)$$

and for $m \geq 2$

$$\theta_i^{(m+1)} = \theta_{MT}^{(m+1)} + \eta p_i^m(\theta_{base}, \dots, \theta_{MT}^{(m)}) - \frac{\eta^2}{2} s_i^{m-1}(\theta_{base}, \dots, \theta_{MT}^{(m-1)}) + O(\eta^3) \quad (17)$$

Proof. We first show that the statement is true for $m = 1$, and then prove the results for $m \geq 2$ by induction. In this case, the base case is given for $m = 2$. In the induction step, instead, we prove that if the statement holds for any given case m then it must also hold for the next case $m + 1$.

$m = 1$. **First epoch** For each task $i = 1, \dots, |T|$

$$\theta_i^{(1)} = \theta_{\text{base}} - \eta \nabla \bar{L}_i(\theta_{\text{base}}) \text{ while } \theta_{\text{MT}}^{(1)} = \theta_{\text{base}} - \alpha \eta \sum_{i \in T} \nabla \bar{L}_i(\theta_{\text{base}}).$$

Consequently, it holds that

$$\begin{aligned} \theta_i^1 &= \theta_{\text{MT}}^{(1)} + \eta \left[\alpha \sum_{j \neq i} \nabla \bar{L}_j(\theta_{\text{base}}) + (\alpha - 1) \nabla \bar{L}_i(\theta_{\text{base}}) \right] \\ &= \theta_{\text{MT}}^{(1)} + \eta r_i(\theta_{\text{base}}) = \theta_{\text{MT}}^{(1)} + \eta p_i^0(\theta_{\text{base}}). \end{aligned}$$

$m = 2$. **Second epoch**

$$\begin{aligned} \theta_i^{(2)} &= \theta_i^{(1)} - \eta \nabla \bar{L}_i(\theta_i^{(1)}) \\ &= \theta_{\text{MT}}^{(1)} + \eta r_i(\theta_{\text{base}}) - \eta \nabla \bar{L}_i \left(\theta_{\text{MT}}^{(1)} + \eta r_i(\theta_{\text{base}}) \right) \\ &\stackrel{\text{Taylor}}{\approx} \theta_{\text{MT}}^{(1)} + \eta r_i(\theta_{\text{base}}) - \eta \nabla \bar{L}_i(\theta_{\text{MT}}^{(1)}) - \frac{\eta^2}{2} \nabla^2 \bar{L}_i(\theta_{\text{MT}}^{(1)}) r_i(\theta_{\text{base}}) + O(\eta^3) \\ &= \theta_{\text{MT}}^{(1)} - \eta \nabla \bar{L}_i(\theta_{\text{MT}}^{(1)}) + \eta r_i(\theta_{\text{base}}) - \frac{\eta^2}{2} \nabla^2 \bar{L}_i(\theta_{\text{MT}}^{(1)}) r_i(\theta_{\text{base}}) + O(\eta^3) \\ &= \theta_{\text{MT}}^{(1)} - \eta \nabla \bar{L}_i(\theta_{\text{MT}}^{(1)}) + \eta \alpha \sum_{t \in T} \nabla \bar{L}_i(\theta_{\text{MT}}^{(1)}) - \eta \alpha \sum_{t \in T} \nabla \bar{L}_i(\theta_{\text{MT}}^{(1)}) + \eta r_i(\theta_{\text{base}}) \\ &\quad - \frac{\eta^2}{2} \nabla^2 \bar{L}_i(\theta_{\text{MT}}^{(1)}) r_i(\theta_{\text{base}}) + O(\eta^3) \\ &= \theta_{\text{MT}}^{(1)} + \eta r_i(\theta_{\text{MT}}^{(1)}) + \eta r_i(\theta_{\text{base}}) - \frac{\eta^2}{2} \nabla^2 \bar{L}_i(\theta_{\text{MT}}^{(1)}) r_i(\theta_{\text{base}}) + O(\eta^3) \\ &= \theta_{\text{MT}}^1 + \eta p_i^1(\theta_{\text{base}}, \dots, \theta_{\text{MT}}^{(1)}) - \frac{\eta^2}{2} s_i^0(\theta_{\text{base}}) + O(\eta^3) \end{aligned}$$

Inductive step Let us assume that

$$\theta_i^{(m)} = \theta_{\text{MT}}^{(m)} + \eta p_i^{m-1}(\theta_{\text{base}}, \dots, \theta_{\text{MT}}^{(m-1)}) - \frac{\eta^2}{2} s_i^{m-2}(\theta_{\text{base}}, \dots, \theta_{\text{MT}}^{(m-2)}) + O(\eta^3)$$

We can derive that

$$\begin{aligned} \theta_i^{(m+1)} &= \theta_i^{(m)} - \eta \nabla \bar{L}_i(\theta_i^{(m)}) \\ &= \theta_{\text{MT}}^{(m)} + \eta p_i^{m-1}(\theta_{\text{base}}, \dots, \theta_{\text{MT}}^{(m-1)}) - \frac{\eta^2}{2} s_i^{m-2}(\theta_{\text{base}}, \dots, \theta_{\text{MT}}^{(m-2)}) - \eta \nabla \bar{L}_i(\theta_i^{(m)}) + O(\eta^3) \\ &= \theta_{\text{MT}}^{(m)} + \eta p_i^{m-1}(\theta_{\text{base}}, \dots, \theta_{\text{MT}}^{(m-1)}) - \frac{\eta^2}{2} s_i^{m-2}(\theta_{\text{base}}, \dots, \theta_{\text{MT}}^{(m-2)}) \\ &\quad - \eta \nabla \bar{L}_i \left(\theta_{\text{MT}}^{(m)} + \eta p_i^{m-1}(\theta_{\text{base}}, \dots, \theta_{\text{MT}}^{(m-1)}) - \frac{\eta^2}{2} s_i^{m-2}(\theta_{\text{base}}, \dots, \theta_{\text{MT}}^{(m-2)}) \right) + O(\eta^3) \\ &= \theta_{\text{MT}}^{(m)} + \eta p_i^{m-1}(\theta_{\text{base}}, \dots, \theta_{\text{MT}}^{(m-1)}) - \frac{\eta^2}{2} s_i^{m-2}(\theta_{\text{base}}, \dots, \theta_{\text{MT}}^{(m-2)}) \\ &\quad - \eta \nabla \bar{L}_i(\theta_{\text{MT}}^{(m)}) - \frac{\eta}{2} \nabla^2 \bar{L}_i(\theta_{\text{MT}}^{(m)}) \left(\eta p_i^{m-1}(\theta_{\text{base}}, \dots, \theta_{\text{MT}}^{(m-1)}) - \frac{\eta^2}{2} s_i^{m-2}(\theta_{\text{base}}, \dots, \theta_{\text{MT}}^{(m-2)}) \right) + O(\eta^3) \\ &= \theta_{\text{MT}}^{(m)} + \eta p_i^{m-1}(\theta_{\text{base}}, \dots, \theta_{\text{MT}}^{(m-1)}) - \frac{\eta^2}{2} s_i^{m-2}(\theta_{\text{base}}, \dots, \theta_{\text{MT}}^{(m-2)}) \\ &\quad - \eta \nabla \bar{L}_i(\theta_{\text{MT}}^{(m)}) - \frac{\eta^2}{2} \nabla^2 \bar{L}_i(\theta_{\text{MT}}^{(m)}) p_i^{m-1}(\theta_{\text{base}}, \dots, \theta_{\text{MT}}^{(m-1)}) + O(\eta^3) \\ &= \theta_{\text{MT}}^{(m+1)} + \eta p_i^m(\theta_{\text{base}}, \dots, \theta_{\text{MT}}^{(m)}) - \frac{\eta^2}{2} s_i^{m-1}(\theta_{\text{base}}, \dots, \theta_{\text{MT}}^{(m-1)}) + O(\eta^3) \end{aligned}$$

□

Proof Theorem and Corollary. For the first epoch

$$\theta_{\text{TA}}^{(1)} = \theta_{\text{base}} + \alpha \sum_{i \in T} \tau_i^{(1)} = \theta_{\text{base}} - \eta \alpha \sum_{i \in T} \nabla \bar{L}_i(\theta_{\text{base}})$$

while, choosing $\alpha\eta$ as learning rate for the loss $\sum_{i \in T} \bar{L}_i$:

$$\theta_{\text{MT}}^{(1)} = \theta_{\text{base}} - \alpha\eta \sum_{i \in T} \nabla \bar{L}_i(\theta_{\text{base}}).$$

So $\theta_{\text{MT}}^{(1)} = \theta_{\text{TA}}^{(1)}$.

For $k \geq 2$, notice that

$$\theta_{\text{MT}}^{(k)} = \theta_{\text{base}} - \alpha\eta \sum_{j=0}^{k-1} \nabla \sum_{t \in T} \bar{L}_i(\theta_{\text{MT}}^{(j)}). \quad (18)$$

Now, using Lemma A.1, we get:

$$\begin{aligned} & -\alpha\eta \sum_{j=0}^{k-1} \nabla \sum_{t \in T} \bar{L}_t(\theta_{\text{MT}}^{(j)}) + \eta p_i^{k-1}(\eta^0, \dots, \eta_{\text{MT}}^{k-1}) \\ &= -\alpha\eta \sum_{j=0}^{k-1} \nabla \sum_{t \in T} \bar{L}_t(\theta_{\text{MT}}^{(j)}) + \sum_{j=0}^{k-1} r_i(\theta_{\text{MT}}^{(j)}) \\ &= -\alpha\eta \sum_{j=0}^{k-1} \nabla \sum_{t \in T} \bar{L}_i(\theta_{\text{MT}}^{(j)}) + \sum_{j=0}^{k-1} \alpha \sum_{j \in T} \nabla \bar{L}_j(\theta_{\text{MT}}^{(j)}) - \nabla \bar{L}_i(\theta_{\text{MT}}^{(j)}) \\ &= -\eta \sum_{j=0}^{k-1} \nabla \bar{L}_i(\theta_{\text{MT}}^{(j)}). \end{aligned}$$

Namely:

$$\begin{aligned} \theta_i^{(m+1)} &= \theta_{\text{MT}}^{(m+1)} + \eta p_i^m(\theta_{\text{base}}, \dots, \theta_{\text{MT}}^{(m)}) - \frac{\eta^2}{2} s_i^{m-1}(\theta_{\text{base}}, \dots, \theta_{\text{MT}}^{(m-1)}) + O(\eta^3) \\ &= \theta_{\text{base}} - \alpha\eta \sum_{j=0}^m \nabla \sum_{t \in T} \bar{L}_i(\theta_{\text{MT}}^{(j)}) + \eta p_i^m(\theta_{\text{base}}, \dots, \theta_{\text{MT}}^{(m)}) - \frac{\eta^2}{2} s_i^{m-1}(\theta_{\text{base}}, \dots, \theta_{\text{MT}}^{(m-1)}) + O(\eta^3) \\ &= \theta_{\text{base}} - \eta \sum_{j=0}^m \nabla \bar{L}_i(\theta_{\text{MT}}^{(j)}) - \frac{\eta^2}{2} s_i^{m-1}(\theta_{\text{base}}, \dots, \theta_{\text{MT}}^{(m-1)}) + O(\eta^3) \end{aligned}$$

we can rewrite the tasks vectors as

$$\tau_i^{(k)} = \theta_i^{(k)} - \theta_{\text{base}} \quad (19)$$

$$= -\eta \sum_{j=0}^{k-1} \nabla \bar{L}_i(\theta_{\text{MT}}^{(j)}) - \frac{\eta^2}{2} s_i^{k-2}(\theta_{\text{base}}, \dots, \theta_{\text{MT}}^{(k-2)}) + O(\eta^3) \quad (20)$$

Consequently the model obtained with TA is

$$\begin{aligned}
\theta_{\text{TA}}^{(k)} &= \theta_{\text{base}} + \alpha \sum_{i \in T} \tau_i^{(k)} \\
&= \theta_{\text{base}} - \eta \alpha \sum_{j=0}^{k-1} \sum_{i \in T} \nabla \bar{L}_i(\theta_{\text{MT}}^{(j)}) - \alpha \sum_{i \in T} \frac{\eta^2}{2} s_i^{k-2}(\theta_{\text{base}}, \dots, \theta_{\text{MT}}^{(k-2)}) + O(\eta^3) \\
&= \theta_{\text{MT}}^{(k)} - \alpha \sum_{i \in T} \frac{\eta^2}{2} s_i^{k-2}(\theta_{\text{base}}, \dots, \theta_{\text{MT}}^{(k-2)}) + O(\eta^3).
\end{aligned}$$

□

A.2 UPPER BOUNDING THE MULTI-TASK LOSS

In this section, we explore the relationship between the PA-ATM loss, defined as the mean of average losses over all tasks, and the loss of a model trained jointly on all the datasets. We conduct this analysis using GD, rather than SGDs, thus removing stochasticity and enabling a clearer analysis while retaining the key insights. Denoting with t both the task and its corresponding dataset with cardinality n_t . The total number of samples for all tasks is given by $N = \sum_{t \in T} n_t$.

By Theorem 1, when merging occurs after one step of finetuning on each dataset, the PA-ATM update is given by:

$$\theta_{\text{base}}^{(k+1)} = \theta_{\text{base}}^{(k)} + \frac{\alpha}{|T|} \sum_{t \in T} \tau_t^{(k)} = \theta_{\text{base}}^{(k)} - \alpha \eta \nabla \left(\frac{1}{|T|} \sum_{t \in T} \bar{L}_t \right), \quad (21)$$

which corresponds to performing a GD step over the loss $L_{\text{ATM}} = \frac{1}{|T|} \sum_{t \in T} \bar{L}_t$.

Having established that one step of PA-ATM in GD minimizes $L_{\text{PA-ATM}}$, a crucial question arises: under what conditions does minimizing L_{ATM} imply the minimization of L_{target} ? In other words, when can we be certain that optimizing the PA-ATM loss will also minimize the loss associated with training jointly on all datasets?

To study if optimizing the PA-ATM loss will also minimize the loss associated with training jointly on all datasets we first note that $L_{\text{PA-ATM}}$ is an unweighted average of the individual dataset losses, while the target loss is a weighted average:

$$L_{\text{target}}(\theta) = \frac{\sum_{t \in T} n_t \bar{L}_t(\theta)}{\sum_{t \in T} n_t}. \quad (22)$$

We now analyze the parameter update from $\theta^{(k)}$ to $\theta^{(k+1)}$. For both PA-ATM and target methods, we denote the change in loss, L_{method} , as $\Delta L_{\text{method}} = L_{\text{method}}(\theta^{(k)}) - L_{\text{method}}(\theta^{(k+1)})$. In the following theorem, we prove that if the drop in ATM loss exceeds a threshold δ , the target loss will also decrease. The value of δ depends on the size of the largest dataset with a decreasing loss and the smallest dataset with an increasing loss. In particular, if the former dataset is larger than the latter, a reduction in PA-ATM loss reduces the target loss. In practice, this is ensured when the loss is reduced on the largest dataset.

Theorem 2. Let $D = \{t \mid \Delta \bar{L}_t > 0\}$ be the set of datasets where the loss decreases after a parameter update, and $I = \{t \mid \Delta \bar{L}_t \leq 0\}$ be the set of datasets where the loss increases or remains unchanged. If the reduction in the PA-ATM loss satisfies $\Delta L_{\text{PA-ATM}} > \delta$, where

$$\delta = \frac{1}{|T|} \left(1 - \frac{\min_{t \in I} n_t}{\max_{t \in D} n_t} \right) \sum_{t \in I} |\Delta \bar{L}_t|,$$

then the target loss L_{target} will also decrease, i.e., $\Delta L_{\text{target}} > 0$.

Proof. Suppose that when transitioning from parameters $\theta^{(i)}$ to parameters $\theta^{(i+1)}$, the change in the average loss for each dataset D_k is given by $\Delta \bar{L}_k = \bar{L}_k(\theta^{(i)}) - \bar{L}_k(\theta^{(i+1)})$. We denote by P the set

of tasks for which the delta of the loss is positive and by P the set for which it is negative, namely $P = \{k \in T \text{ s.t. } \Delta \bar{L}_k > 0\}$ and $N = \{k \in T \text{ s.t. } \Delta \bar{L}_k \leq 0\}$. The set $\{1, \dots, n\} = P \cup N$. In the following formulas we will use the symbol $|\cdot|$ for different purposes. For sets, like D_i , $|D_i|$ denotes the cardinality of the set, while for scalars, such as $\Delta \bar{L}_k$, $|\Delta \bar{L}_k|$ denotes their absolute value. Since the tasks in N have negative $\Delta \bar{L}_k$, it holds that

$$\sum_{j \in N} |D_j| \Delta \bar{L}_j = - \sum_{j \in N} |D_j| |\Delta \bar{L}_j|.$$

Under the hypothesis that $\Delta L_{\text{PA-ATM}} > \delta$, this implies $\sum_{j=1}^n \Delta_j > n\delta$. We have that $\sum_{j \in P} \Delta \bar{L}_j + \sum_{j \in N} \Delta \bar{L}_j = \sum_{j \in P} \Delta \bar{L}_j - \sum_{j \in N} |\Delta \bar{L}_j| > n\delta$, namely $\sum_{j \in P} \Delta \bar{L}_j > n\delta + \sum_{j \in N} |\Delta \bar{L}_j|$.

We want to prove that $\Delta L_{\text{target}} > 0$. Let us now consider $\Delta L_{\text{target}} > 0$ iff $\sum_{j=1}^n |D_j| \Delta_j > 0$.

$$\begin{aligned} \sum_{j=1}^n |D_j| \Delta_j &= \sum_{j \in P} |D_j| \Delta \bar{L}_j + \sum_{j \in N} |D_j| \Delta \bar{L}_j \\ &= \sum_{j \in P} |D_j| \Delta \bar{L}_j - \sum_{j \in N} |D_j| |\Delta \bar{L}_j| \\ &> \min_{j \in P} |D_j| \sum_{j \in P} \Delta \bar{L}_j - \max_{j \in N} |D_j| \sum_{j \in N} |\Delta \bar{L}_j| \\ &> \min_{j \in P} |D_j| \left[n\delta + \sum_{j \in N} |\Delta \bar{L}_j| \right] - \max_{j \in N} |D_j| \sum_{j \in N} |\Delta \bar{L}_j| \\ &= n \min_{j \in P} |D_j| \delta + (\min_{j \in P} |D_j| - \max_{j \in N} |D_j|) \sum_{j \in N} |\Delta \bar{L}_j|. \end{aligned}$$

The last line of the previous equation is positive by hypothesis, since we assumed $\delta > \frac{1}{n} (1 - \frac{\min_{j \in N} |D_j|}{\max_{j \in P} |D_j|}) \sum_{j \in N} |\Delta \bar{L}_j|$. \square

Remark 2. If we choose the target loss to be the maximum of the average loss across all datasets $L_{\text{target}} = \max_{t \in T} \bar{L}_t$, by leveraging the equivalence between the L_1 -norm and the max norm, we obtain the bound $L_{\text{target}} \leq T \cdot L_{\text{PA-ATM}}$.

B ADDITIONAL RESULTS

B.1 FULL RESULTS OVER VARYING COMPUTATIONAL BUDGET

In the main paper, we pictorially illustrated the multi-task accuracy of the baselines and ATM variants, in the form of radar plots. For deeper analysis, here we report the full results of PA-ATM and PH-ATM compared to the baselines, as the computational budget K varies across 2, 4, 6, 8, and 10 epochs. Again, we point out that, unlike PA-ATM and the baselines, PH-ATM is finetuned only with validation data. See Table 2.

B.2 FULL RESULTS OF VARYING ATM BUDGET DISTRIBUTION

We show the full accuracy results as we vary the distribution of 10 epochs into different numbers of ATM iterations. See Table 3.

C TASK DIFFICULTY RELATED TO EPOCHS

To gain further insight into *when* finetuning for more epochs might offer advantages in Task Arithmetic (TA), we examined correlations between task “difficulty” and the difference in merged performance under two settings.

K	Method	Cars	DTD	EuroSAT	GTSRB	MNIST	RESISC45	SVHN	SUN397	Average
2	Task Arithmetic	0.68	0.50	0.81	0.62	0.95	0.74	0.78	0.68	0.72
	TIES	0.75	0.46	0.52	0.44	0.57	0.66	0.52	0.66	0.57
	Breadcrumbs	0.68	0.50	0.80	0.61	0.95	0.74	0.77	0.68	0.72
	DARE	0.68	0.50	0.81	0.62	0.95	0.74	0.78	0.68	0.72
	PA-ATM	0.71	0.53	0.90	0.75	0.98	0.78	0.86	0.70	0.78
4	Task Arithmetic	0.69	0.49	0.79	0.63	0.96	0.74	0.78	0.68	0.72
	TIES	0.80	0.46	0.53	0.45	0.58	0.66	0.50	0.65	0.58
	DARE	0.68	0.49	0.79	0.63	0.96	0.74	0.78	0.68	0.72
	Breadcrumbs	0.68	0.49	0.79	0.62	0.96	0.73	0.77	0.68	0.76
	PA-ATM	0.74	0.59	0.95	0.90	0.99	0.84	0.93	0.72	0.83
6	Task Arithmetic	0.69	0.49	0.80	0.64	0.96	0.74	0.79	0.68	0.72
	TIES	0.82	0.45	0.50	0.45	0.57	0.66	0.51	0.65	0.58
	DARE	0.69	0.49	0.80	0.63	0.96	0.74	0.79	0.68	0.72
	Breadcrumbs	0.69	0.48	0.79	0.63	0.96	0.73	0.77	0.68	0.72
	PA-ATM	0.77	0.64	0.97	0.95	0.99	0.87	0.95	0.74	0.86
8	Task Arithmetic	0.70	0.49	0.79	0.65	0.96	0.73	0.78	0.68	0.72
	TIES	0.83	0.46	0.52	0.45	0.60	0.66	0.49	0.65	0.58
	DARE	0.69	0.49	0.79	0.64	0.96	0.73	0.79	0.68	0.72
	Breadcrumbs	0.69	0.49	0.79	0.64	0.96	0.73	0.77	0.68	0.72
	PA-ATM	0.78	0.67	0.98	0.96	0.99	0.89	0.96	0.74	0.87
10	Task Arithmetic	0.69	0.49	0.80	0.64	0.97	0.73	0.79	0.68	0.72
	TIES	0.83	0.46	0.52	0.44	0.60	0.65	0.51	0.65	0.58
	DARE	0.68	0.49	0.80	0.63	0.97	0.73	0.79	0.68	0.72
	Breadcrumbs	0.69	0.49	0.80	0.64	0.97	0.73	0.77	0.68	0.72
	PA-ATM	0.79	0.69	0.98	0.97	0.99	0.90	0.96	0.75	0.88

Table 2: ATM vs. Baselines as budget varies (*ViT-B-16*)

Iterations	Epochs/iteration	Cars	DTD	EuroSAT	GTSRB	MNIST	RESISC45	SVHN	SUN397	Average
1	10	0.6886	0.4858	0.8027	0.6402	0.9681	0.7276	0.7850	0.6792	0.7222
2	5	0.7203	0.5337	0.9093	0.8004	0.9862	0.7857	0.8971	0.6964	0.7911
5	2	0.7668	0.6126	0.9616	0.9395	0.9921	0.8716	0.9494	0.7279	0.8527
10	1	0.7904	0.6897	0.9837	0.9713	0.9943	0.9032	0.9644	0.7490	0.8808

Table 3: PA-ATM accuracies for different budget distributions

Specifically, we tracked both loss and accuracy at the first and last epochs during finetuning. For each task, we then derived four key metrics:

$$\begin{aligned}
\text{acc_gap} &= \text{acc}_{\text{last}} - \text{acc}_{\text{first}}, \\
\text{acc_ratio} &= \frac{\text{acc}_{\text{first}}}{\text{acc}_{\text{last}}}, \\
\text{loss_gap} &= \text{loss}_{\text{first}} - \text{loss}_{\text{last}}, \\
\text{normalized_loss_gap} &= \frac{\text{loss_gap}}{\text{loss}_{\text{first}}}.
\end{aligned}$$

Intuitively, tasks showing smaller loss_gap or acc_gap can be viewed as “easier” relative to the pre-trained initialization, whereas larger gaps indicate a need for more substantial finetuning to reach high accuracy.

Next, we sampled approximately 800 distinct five-task subsets drawn from the twenty tasks used in (Gargiulo et al., 2024), merged the individual fine-tuned models using both single-epoch TA (1 EPOCH) and vanilla TA, and measured the average test accuracy of each merged model.

From Figure 9, some key observations arise. For “easier” tasks, characterized by smaller acc_gap or loss_gap , the difference Δavg is close to zero, indicating that single-epoch TA typically matches or comes very close to vanilla TA. In such settings, the tasks do not heavily diverge from the pretrained representation, and simpler merging strategies appear sufficient. For “harder” tasks, where acc_gap or loss_gap is larger, we observe that Δavg tends to be negative, favoring vanilla TA. Here, specialized finetuning steps seem more crucial, giving an edge to vanilla TA in preserving task-specific refinements within the merged model.

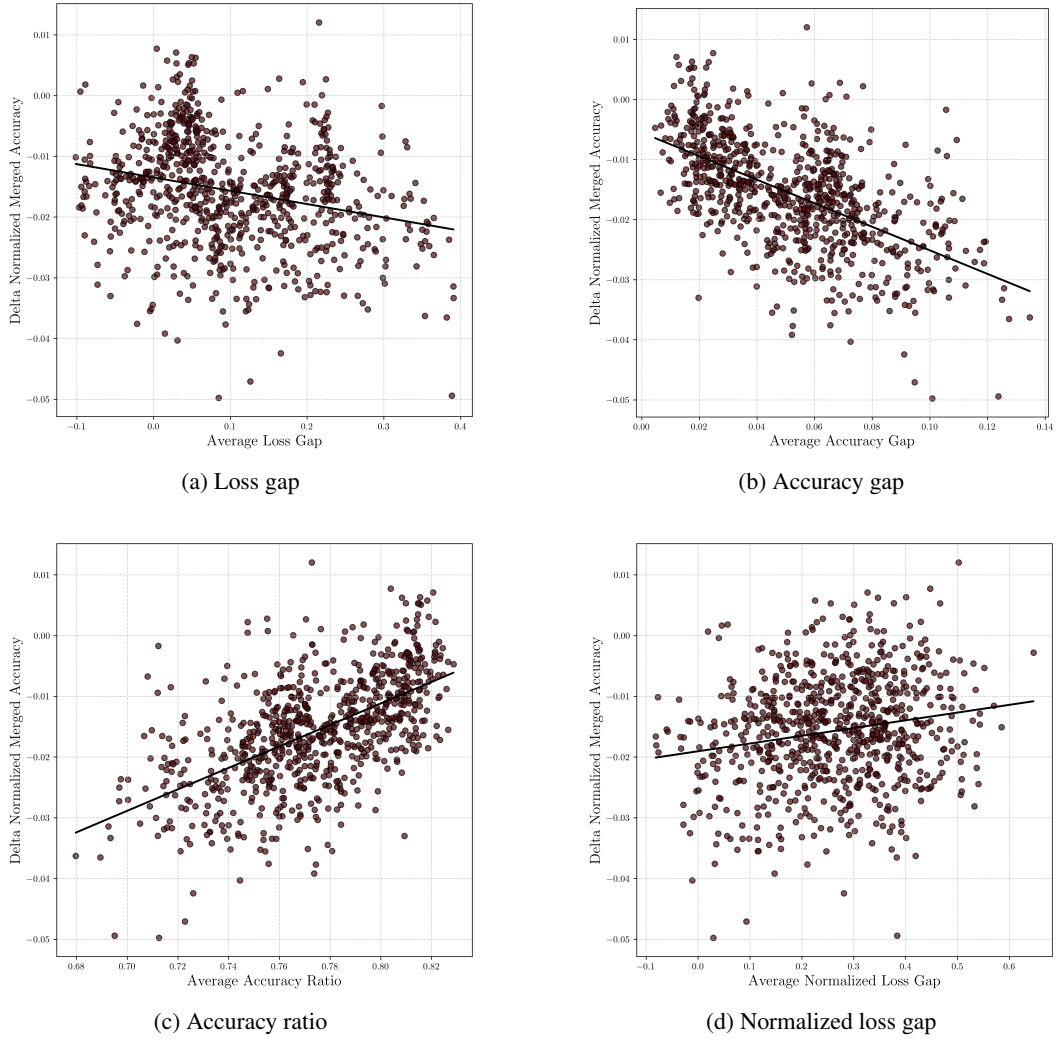


Figure 9: Visualization of task difficulty metrics against delta of normalized merged accuracy.

Overall, these findings suggest that while vanilla TA or standard multi-task approaches may be more suitable for especially challenging tasks (i.e. those requiring extensive finetuning to reach high accuracy), single-epoch TA is appealing in budget-critical settings or when tasks are relatively straightforward to learn from a pretrained model. In practice, one can anticipate slightly better results from vanilla TA for tasks that significantly diverge from the pretrained initialization, but benefit from single-epoch TA due to less finetuning.